J Sol-Gel Sci Technol (2010) 53:543–550
DOI 10.1007/s10971-009-2129-5

ORIGINAL PAPER

Detection of up-conversion in nano-structure $BaTiO_3$ co-doped with Er^{3+} and Yb^{3+} ions

I. K. Battisha · Y. Badr · N. M. Shash · M. G. El-Shaarawy · A. G. A. Darwish

Received: 16 December 2008 / Accepted: 4 December 2009 / Published online: 27 January 2010

Abstract Nano-structure pure barium titanate $BaTiO_3$ (BT) and (BT) co-doped with constant concentration of Er^{3+} ions and different concentrations of Yb^{3+} ions were prepared using sol–gel method. XRD results confirmed that the pure sample was found to crystallize in tetragonal phase by sintering at 750 °C for 1 h. All major peaks corresponding to perovskite BT phase appeared. Efficient infrared-to-visible up-conversion is reported in the doped samples. The conversion process and results in the generation of visible emissions are discussed. Up-conversion efficiency for red emission predominates in doped samples. Results illustrate the large potential of this class of materials for photonic applications in optoelectronics devices.

Keywords Sol–gel · Powders · Thin films · Up-conversion · BaTiO3 nano-crystals · Er^{3+}: Yb^{3+} ions

1 Introduction

Near-infrared to visible up-conversion is an important approach for the generation of visible luminescence and short wavelength laser actions. Recently, the interest in up-conversion emission has been increased due to the needs for all-solid compact laser devices operating in the blue-green region and the availability of powerful near-infrared GaAs/(Al, Ga) as laser diodes that can be used in such systems. Furthermore, the availability of very efficient up-conversion systems may lead to novel devices such as infrared light detection, new displays and lighting [1–9]. Some rare earth doped $BaTiO_3$ films have been prepared, their structural, physicochemical, optimization, characterization, understanding of luminescence, optical up-conversion mechanisms, and the size effects were investigated and lasing emissions have also been studied [10–19]. But so far, there has been rare report on the up-conversion of co-doped $BaTiO_3$ with Er^{3+} and Yb^{3+} ions. The far reaching strategic goals of the work relate to the development of a new technology implemented through the synthesis of novel nano-structured materials exhibiting advanced light emission functionality and the study and exploitation of novel fundamental effects. The objective of the present work is to develop nano-structured ferroelectric $BaTiO_3$ (BT), in the form of powder and thin film, doped with well-dispersed erbium and ytterbium ions with different concentrations, all prepared by sol–gel technique. The structure and optical properties will be evaluated using XRD, and photoluminescence analysis.

I. K. Battisha (✉) · A. G. A. Darwish
Department of Solid State Physics, National Research Center (NRC), Dokky, Giza, Egypt
e-mail: szbasha@yahoo.com

Y. Badr
National Institute of Laser Enhancement Sciences (NILES), Cairo University, Cairo, Egypt

N. M. Shash · M. G. El-Shaarawy
Faculty of Science, Physics Department, Banha University, Banha, Egypt

2 Experimental

2.1 Preparation

Pure $BaTiO_3$ (BT) in powder form, and doped with different concentrations of Er $(NO_3)_3$-H_2O (BT1E, BT3E and BT5E), and co-doped with constant concentration 4% of Er $(NO_3)_3$-H_2O and different concentrations of Yb

$(NO_3)_3$-H_2O^{3+} (at 1, 3, and 5% of Yb^{3+} ions) (BT4E1Y), (BT4E3Y) and (BT4E5Y), respectively, were prepared by a modified sol–gel method, Table 1 shows the composition of the prepared powder samples. Barium acetate ($Ba(Ac)_2$) (99%, Sisco Research Laboratories PVT.LTD, India) and titanium butoxide ($Ti(C_4H_9O)_4$), (97%, Sigma–Aldrich, Germany) were used as the starting materials; acetyl acetone (AcAc, $C_5H_8O_2$), (98%, Fluka, Switzerland) acetic acid (HAc)-H_2O mixture (96%, Adwic, Egypt) were adopted as solvents of ($Ti(C_4H_9O)_4$), and $Ba(Ac)_2$, respectively. Er $(NO_3)_3$-H_2O and Yb $(NO_3)_3$-H_2O (99.9%, Aldrich), solutions were added to the precursor with different molar ratios. The solutions were kept in air at room temperature, yielding transparent solutions.

Dry gels obtained by baking the gel at 130 °C, were sintered at heat treatment temperature 750 °C for 1 h, in a muffle furnace type (Carbolite CWF 1200). BT thin film doped with different concentrations of Er $(NO_3)_3$-H_2O at 1–5% (BT1E, BT2E, BT3E, BT4E and BT5E) and BT thin film co-doped with 1% Er $(NO_3)_3$-H_2O and different concentrations of Yb$(NO_3)_3$-H_2O at 2, 4 and 5% (BT4E2YTF, BT4E4YTF and BT4E5YTF,) were prepared by a modified spin coating sol–gel method, Table 2 shows the composition of the prepared thin film samples. The same solutions used in preparing the powder samples were filtered through filter paper and remained stable for 4 days, which was long enough to carry out multiple spin-coating preparations. The final solutions were stirred for another hour before spin coating. All operations were performed at room temperature. Silica substrates were used as substrates for the deposition of nano-structure thin films by spin coating. Solutions were dispersed on the silica glass substrate and then spun at 6000 rev/min for 30 s. At least 15 successive coatings were required to provide suitable film thicknesses. Thin film samples were annealed in air in a conventional oven and sintered at 750 °C for 1 h.

2.2 Characterization

X-ray diffraction (XRD) patterns of the prepared samples were recorded using a Philips X-ray diffractometer provided with monochromatized CuKα1 radiation of wavelength = 1.54056 Å from a fixed source operated at 45 kV and 9 mA. Crystallite sizes G were determined using the Scherrer's equation ($G = K\lambda/D\ \cos\Theta$), where K is the Scherrer constant (0.89), λ is the diffraction for a particular Bragg diffraction peak, and D is the (corrected) full width (in radians) of the peak at half maximum (FWHM) intensity. The correction to the measured FWHM Ds for a sample peak was made to accommodate systemic instrumental broadening and utilized peak widths Dq measured from a diffraction scan, taken under identical conditions, from a strain-free powdered quartz sample, with crystallite size ranging between 5 and 10 μm. The corrected sample peak widths were calculated as $D = (Ds_2 - Dq_2)_{1/2}$, where Ds is the full width of the peak at half maximum (FWHM) intensity of the prepared sample and Dq is of the standard quartz sample. Micro-strain and crystallite size contributions to D were separated using the Win-Fit program, using standard samples for estimation of instrumental broadening. The final sample crystallite sizes G were obtained by Fourier analysis, using the corrected profile. The diffraction peak used was the most intense diffraction peak, assigned to the (110) reflection from the BT powder phase. The excitation and up-conversion emission spectra of the prepared samples were recorded using the chopped laser diode at 808 nm. Incident beam power was 100 mW. The emission was analyzed using Spex 750 M monochromator (Gratting 1200) and detected with a photomultiplier tube. The PL was obtained using lock-in amplifier (SR 510-Stanford) technique and controlled by a suitable soft ware. The measurements were performed at room temperature.

Table 1 Symbols, concentrations and compositions of Er^{3+} and Yb^{3+} ions-doped nano-structure BT powders

Sample symbols and abbreviations	Dopant ions	Formula of composition
BT1E, BT2E, BT3E, BT4E and BT5E; (1, 2, 3, 4, 5 and 15%)	Er^{3+}	$Ba_{1-x}Er_{(x=0.01–0.05)}TiO_{3+\Delta}$ Δ = 0.005, 0.0099, 0.015, 0.0199, 0.024 and 0.065
BT4E1Y, BT4E2Y, BT4E3Y, BT4E4Y and BT4E5Y; (4% Er^{3+} and 1–5% Yb^{3+})	Er^{3+} and Yb^{3+}	$Ba_{0.96}Er_{0.04}Ti_{1-y}Yb_{(y=0.01–0.05)}O_{3+\Delta}$ Δ = 0.0866, 0.0999, 0.11, 0.12 and 0.13

Table 2 Name and concentration of Er^{3+} and Yb^{3+} doped nano-structure BT thin films

Sample symbols and abbreviations	Dopant ions	Formula of composition
BT2ETF, BT4ETF and BT5ETF; (2, 4 and 5%)	Er^{3+}	$Ba_{1-x}Er_{(x=0.02,\ 0.03,\ 0.05)}TiO_{3+\Delta}$ Δ = 0.0099, 0.0199 and 0.024
BT4E2YTF; (4% Er^{3+} and 2, 4 and 5% Yb^{3+})	Er^{3+} and Yb^{3+}	$Ba_{0.96}Er_{0.04}Ti_{1-y}Yb_{(y=0.02,\ 0.04,\ 0.05)}O_{3+\Delta}$ Δ = 0.0999, 0.12 and 0.13

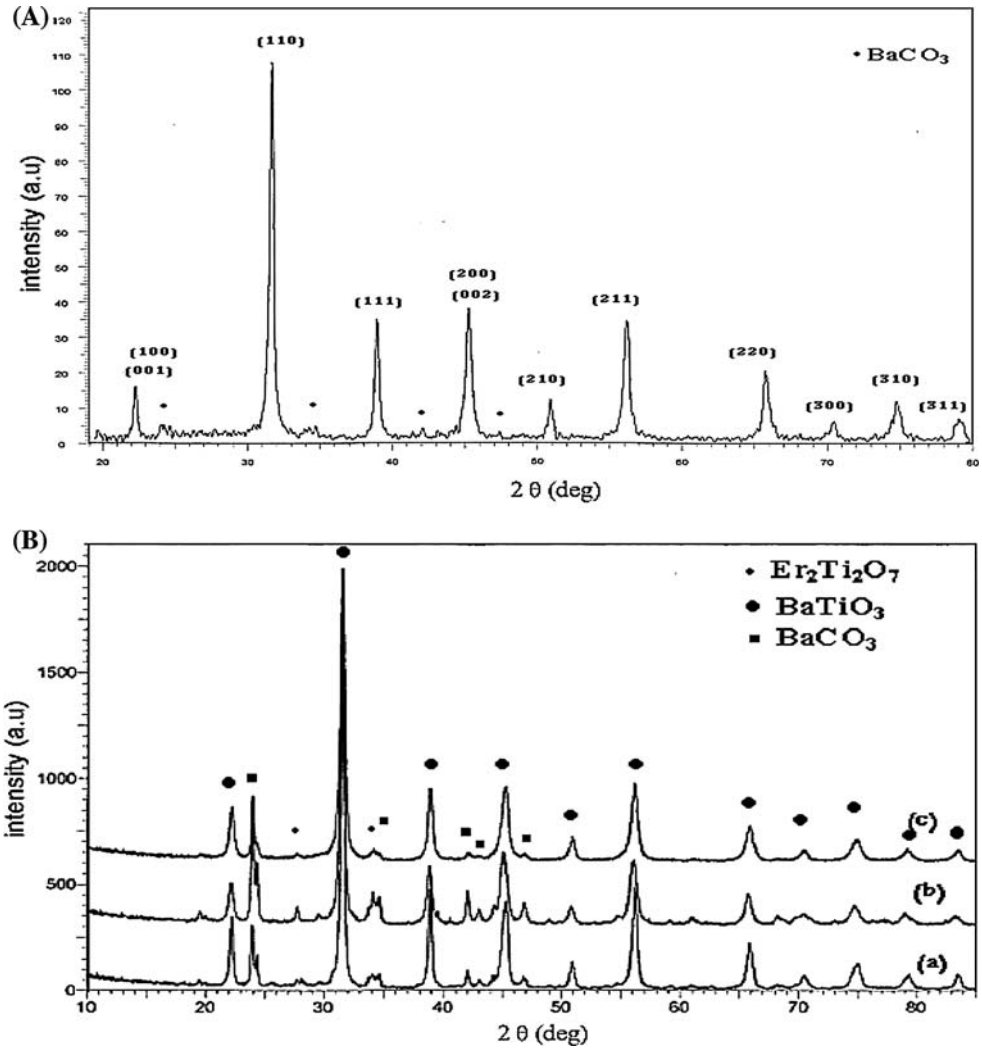

Fig. 1 XRD patterns of **A** pure powder nano-structure BT and **B** BT doped with diff. conc. of Er^{3+} ions (*a*) (BT1E), (*b*) (BT3E) and (*c*) (BT5E), sintered at 750 °C for 1 h

3 Results and discussion

Figure 1A, B shows the XRD patterns of (A) pure BT powder and (B) BT doped with different concentrations of Er^{3+} ions (a) (BT1E), (b) (BT3E), (c) (BT5E), all in powder form, and sintered at 750 °C for 1 h. It is clearly seen that crystallized BT phase can be obtained at heating temperature 750 °C, indicating that one phase tetragonal BT is presented in the prepared pure and doped samples, (referencing to JCPDS files 75-0215 and JCPDS files 79-2265 for pure BT and doped BT, respectively for tetragonal phases), which shows well defined perovskite structure with higher intensity and no detectable secondary phases in the pure BT pattern. The given data in Table 3 showed all the peaks which is corresponding of the tetragonal phase. The splitting of the (001) and (100) doublets confirmed that the prepared powder has a perovskite tetragonal phase. Very low unwanted amount of un-reacted $BaCO_3$ (By reference to JCPDS files 45-1471 for Witherite, syn) resulting from the reaction of BaO with atmospheric CO_2 and the burn-out of organic materials or as a result of incomplete calcinations appeared in both Fig. 1A, B. While the un-wanted amount of $BaCO_3$ was seen in the pure BT sample with a smaller amount. Due to the solubility of Er_2O_3, the doping with different

Table 3 2 Zeta degree against the diffraction line of tetragonal phase of pure BT prepared by sol gel technique in the powder form

2 Zeta degree	Diffraction line of tetragonal phase
22.18	(100)
31.7	(110)
38.9	(111)
45.26	(002)
50.88	(210)
56.27	(211)
65.9	(220)
70.5	(300)
74.87	(310)
79.23	(311)

Table 4 The grain size (nm), tetragonality factor (c/a) and the unit cell volume$(A^0)^3$ of the doped BT powder with different concentrations of Er^{3+} ions, (BT1E), (BT3E), (BT5E)

Dopant name	Grain size (nm)	Tetragonality factor (*c*/*a*)	Unit cell volume $(A^0)^3$
BT1E	37	1.024	64.82
BT3E	44	1.019	65.97
BT5E	38	1.003	64.35

concentrations caused secondary phase or impurity phase of $Er_2Ti_2O_7$ at $2\Theta = 27.66$ and 34.63 indexed as (222) and (400), as shown in Fig. 1B. The analysis of the XRD patterns indicate that the splitting in the (001) and (100) doublets decreases with the increase of Er^{3+} ions concentration indicating a gradual transition from the tetragonal to the cubic and hence a lowering in the tetragonality factor is observed [20]. Table 4 shows the variation of the tetragonality factor *c*/*a* and the unit cell volume as a function of the doping concentration, obtained from our XRD measurements recorded at room temperature.

The tetragonality factor and the unit cell volume were found to decrease with increasing the Er^{3+} ions content, which was observed also for the samples having a constant Er^{3+} ions concentration and different concentrations of Yb^{3+} ions, which exhibit the tetragonal to cubic transition.

Figure 2 shows the XRD patterns for BT3E and JCPDS files for $BaTiO_3$ and $BaCO_3$. By doping nano-structure BT powder with Er^{3+} ions the formation of $BaCO_3$ appears [20]. The effect of co-doping BT with Er^{3+} and Yb^{3+} ions on the structure of BT is shown in Fig. 3, for constant concentration (BT4E) and different concentrations of Yb^{3+} ions at (BT4E1Y, BT4E3Y and BT4E5Y), respectively. The obtained BT phase has also a tetragonal perovskite structure (by reference to JCPDS files 75-2120 for tetragonal phases of the $BaTiO_3$), the impurity phases might be

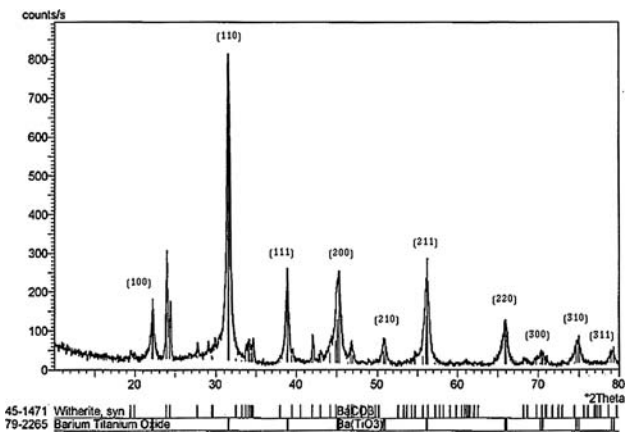

Fig. 2 The XRD patterns for 3% Er^{3+}: $BaTiO_3$ and JCPDS files for $BaTiO_3$ and $BaCO_3$

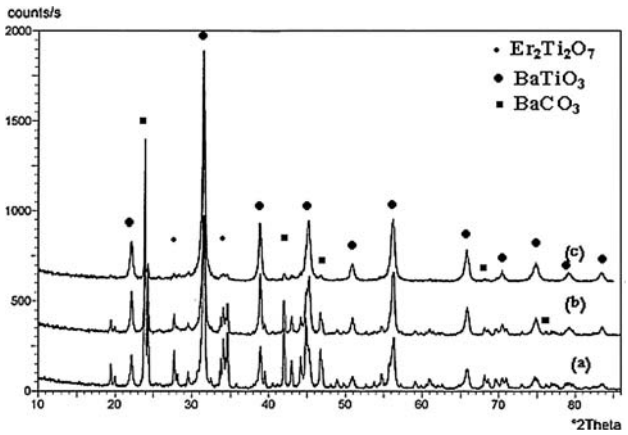

Fig. 3 The XRD patterns of $BaTiO_3$ co-doped with constant concentration at 4% for Er^{3+} ions and different concentrations of Yb^{3+} ions, (*a*) BT4E1Y, (*b*) BT4E3Y and (*c*) BT4E5Y

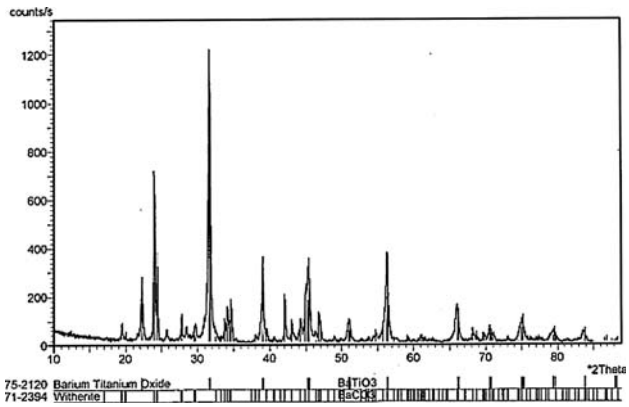

Fig. 4 The XRD patterns for 4% Er and 1% Yb: $BaTiO_3$ and JCPDS files for $BaTiO_3$ and $BaCO_3$

due to the present of the $Er_2Ti_2O_7$ and no observed $Yb_2Ti_2O_7$ phase, while un-wanted amount of un-reacted $BaCO_3$ appeared, (referencing to JCPDS files 71-2394 for Witherite, syn $BaCO_3$), [21]. Figure 4, shows the XRD patterns for (BT4E1Y) doped BT and JCPDS files for $BaTiO_3$ and $BaCO_3$. It is obvious that by co-doping the BT with Er^{3+} and Yb^{3+} ions the formation of $BaCO_3$ also appears. The average crystallite sizes were found to be dependent on the concentrations of erbium, as it decreases from 38 to 37 nm by increasing the concentration of Er^{3+} ions. While for the Er^{3+}, Yb^{3+} co-doped samples the crystallite size decreases from 64 to 54 nm by increasing the concentration of Yb^{3+} ions. These obtained results might be due to the fact that substituting Ba^{2+} ions (radius 1.56) by Er^{3+} ions (radius 1.31) reduces the unit cell volume [6–8] as shown in Tables 4 and 5.

Figure 5 shows the XRD patterns of BT co-doped with Er^{3+} and Yb^{3+} in thin film form (BT1E3YTF). It is clear

Table 5 The grain size (nm), tetragonality factor (c/a) and the unit cell volume$(A^0)^3$ of the co-doped BT powder with constant concentration 4% of Er^{3+} ions and different concentrations of Yb^{3+} ions, BT4E1Y

Dopant name	Grain size (nm)	Tetragonality factor (*c*/*a*)	Unit cell volume $(A)^3$
BT4E1Y	64	1.022	65.79
BT4E3Y	42	1.008	64.72
BT4E5Y	54	1.004	64.70

that crystallized BT phase can be obtained at 750 °C, indicating that one phase tetragonal $BaTiO_3$ is presented in the prepared thin film sample.

3.1 Up-conversion mechanisms

The emission spectrum of Er^{3+} and Yb^{3+} ions embedded in nano-structure powder of BT resulting from excitation of 808 nm (laser diode).

3.1.1 Up-conversion emission of BT: Er^{3+} ions

The up-conversion effect, observed in BT powder doped with different concentrations of Er^{3+} ions (a) (BT1E), (b) (BT3E), (c) (BT4E), (d) (BT5E) and (e) (BT15E) are shown in Fig. 6. While Fig. 7 shows the up-conversion emission spectra from BT thin films doped with different concentrations of Er^{3+} ions, prepared by spin coating sol–gel technique, and sintered at 750 °C for 1 h.

When laser diode is tuned to a strong absorption, $(^4I_{15/2} \rightarrow {}^4I_{9/2})$ of Er^{3+} ions at ($\lambda = 808$ nm), green and red photoluminescence emission assigned to $(^4S_{3/2} \rightarrow {}^4I_{15/2})$ (554 nm), $(^2H_{11/2} \rightarrow {}^4I_{15/2})$ (532 nm) and $(^4F_{9/2} \rightarrow {}^4I_{15/2})$ (635 nm), respectively for powder samples and at 532 and 634 nm for thin film sample assigned to $(^2H_{11/2} \rightarrow {}^4I_{15/2})$ and $(^4F_{9/2} \rightarrow {}^4I_{15/2})$, respectively. It has been well addressed that the green emissions have been attributed to the intra f-f transitions of Er^{3+} ions, where the red emission is attributed to another f-f transition of Er^{3+} ions for both form of samples, respectively as shown in Table 6.

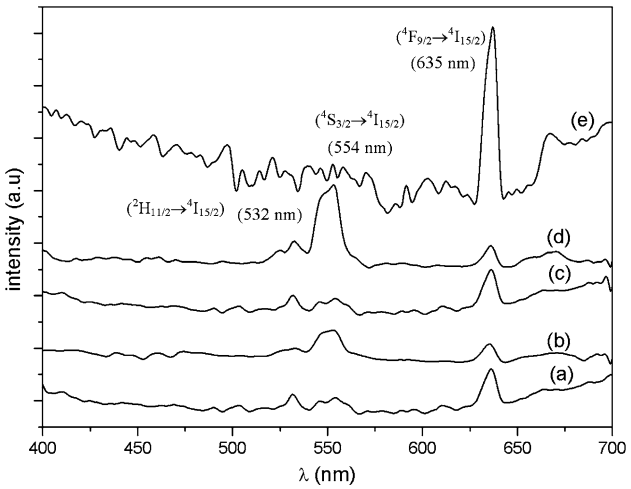

Fig. 6 Up-conversion emission spectra (under 808 nm excitation) from (*a*) (BT1E), (*b*) (BT3E), (*c*) (BT4E), (*d*) (BT5E), (*e*) (BT15E), powder, prepared by sol–gel technique, sintered at 750 °C for 1 h

The peak intensities of the up-conversion emissions were found to increase by increasing the concentration of the erbium ion embedded in the host material up to 4% and then a quenching appeared at 5% of Er^{3+} ions in power samples Nearly the same trend appeared in thin film samples except that the intensity at 5% decreased but still a clear peak appeared with some shift to lower wavelength. It is clearly seen that the visible up-conversion emission peaks of Er^{3+} ions is sharper in the thin film samples.

Figure 8a schematically shows the excited state absorption (ESA) processes of the green emissions of Er^{3+} ions upon excitations at 808 nm. To compare the green and

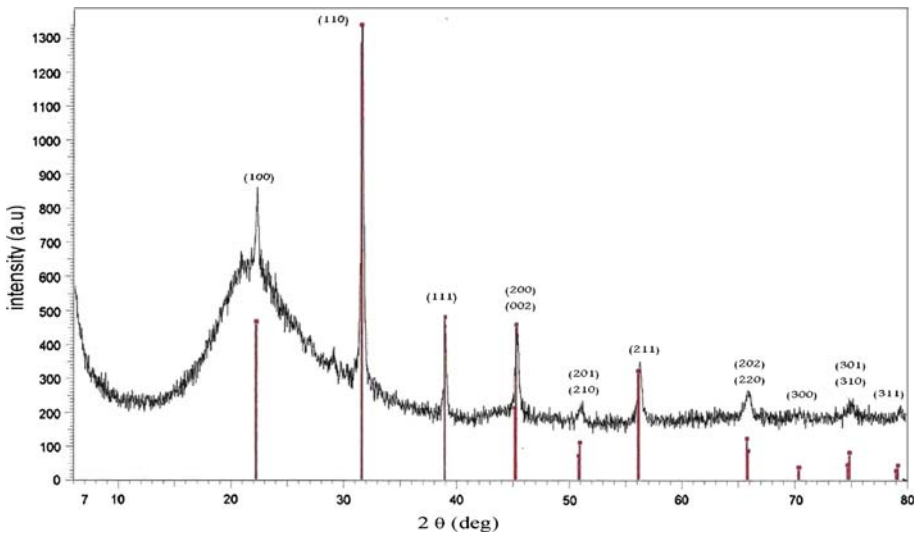

Fig. 5 XRD patterns of $BaTiO_3$ thin film co-doped with 1% Er^{3+} and 3% Yb^{3+} (BT1E3YTF), prepared by sol–gel technique and sintered at 750 °C for 1 h

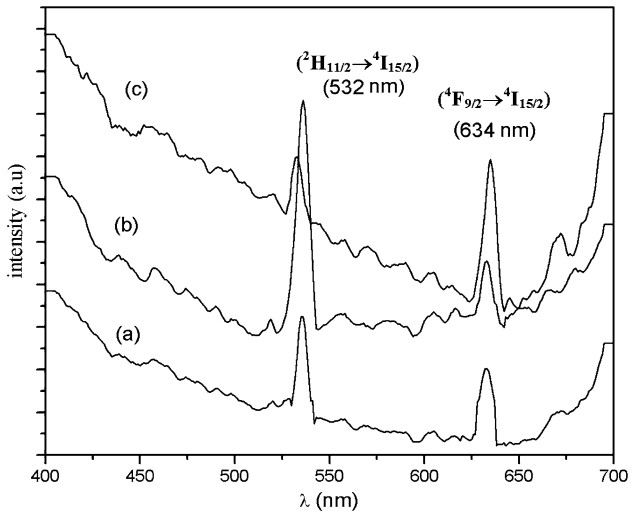

Fig. 7 Up-conversion emission spectra (under 808 nm excitation) from (*a*) (BT2ETF), (*b*) (BT4ETF) and (*c*) (BT5ETF) thin film, prepared by spin coating sol–gel technique, sintered at 750 °C for 1 h

Table 6 The emission bands against the intra f–f transitions of powder and thin film form BT samples doped with Er^{3+} ions

Emission bands positions (nm)	Intra f–f transitions
Powder form	
532	$^2H_{11/2} \rightarrow {}^4I_{151/2}$
554	$^4S_{3/2} \rightarrow {}^4I_{151/2}$
635	$^4F_{97/2} \rightarrow {}^4I_{11/2}$
Thin film form	
532	$^2H_{11/2} \rightarrow {}^4I_{151/2}$
634	$^4F_{97/2} \rightarrow {}^4I_{11/2}$

red up-conversion, we can propose two mechanisms; first one for dominant green luminescence in which, the laser light brings the Er^{3+} ion into $^4I_{9/2}$ level, which then decays through a non-radiative process into the $^4I_{11/2}$ metastable levels and subsequently into the $^4I_{13/2}$ metastable level. Energy transfer processes shown in Fig. 8b bring the Er^{3+} ion into ($^4F_{7/2}$) state from which ($^4S_{3/2}$) is populated through the non-radiative relaxation. The second mechanism is the red luminescence one, which is stronger than the green one in which, the laser beam brings the Er^{3+} ion to the excited state $^4I_{9/2}$ level. One ion nonradiatively decays to the $^4I_{13/2}$ metastable level, and the second decays to the $^4I_{11/2}$ metastable levels. Energy transfer processes bring the Er^{3+} ion to the $^4F_{9/2}$ and a red emission can be

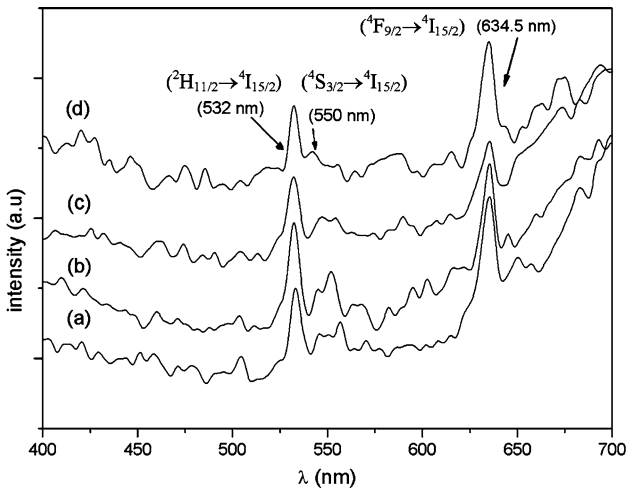

Fig. 9 Up-conversion emission spectra (under 808 nm excitation) for powder samples (*a*) BT4E1Y, (*b*) BT4E2Y, (*c*) BT4E4Y, and (*d*) BT4E5Y

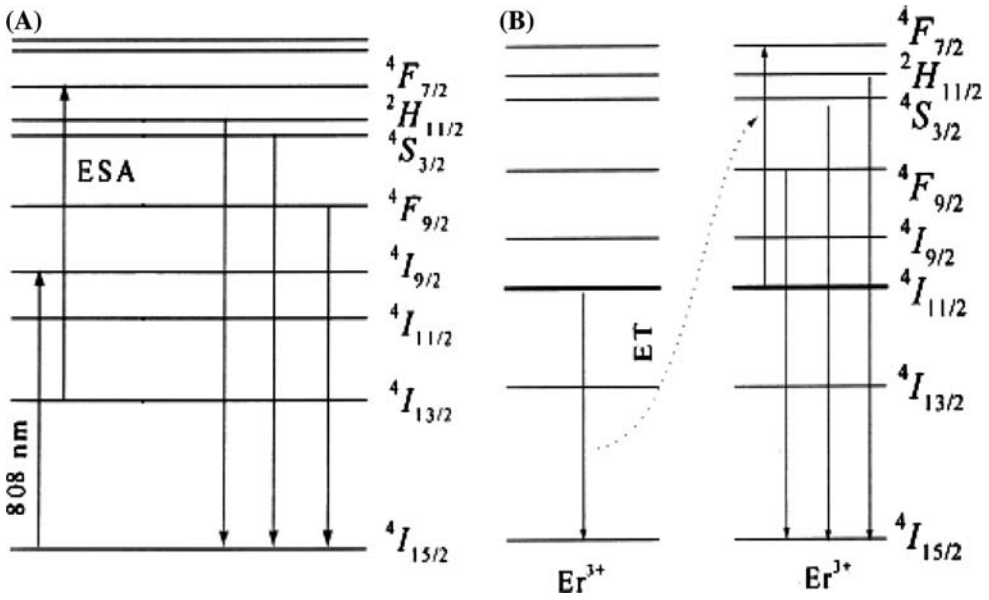

Fig. 8 Schematic diagram of the electronic levels of Er^{3+} ions incorporated into BT in powder and thin film forms, showing the exited state absorption (**a**) and the energy transfer (ET) (**b**) processes for the up-conversion emissions under 808 nm excitations

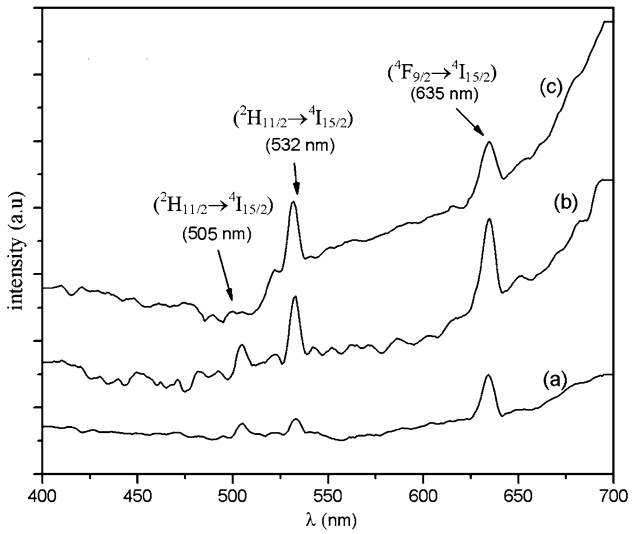

Fig. 10 Up-conversion emission spectra (under 808 nm excitation) for (*a*) BT4E2YTF, (*b*) BT4E4YTF and (*c*) BT4E5YTF thin films, prepared by spin coating sol–gel technique, sintered at 750 °C for 1 h

observed. The spin-allowed radiative transition from the preceding levels to the ground state gives rise to the visible up-conversion emission. The energy transfer (ET) between two close ions also takes place and plays a significant role in the up-conversion emission. However, the much stronger intensity is of red emission, which is observed in thin film (BT3ETF) and in powder samples at all erbium concentrations except for (BT4E). It is expected that the $^4F_{9/2}$ is predominantly excited in these materials, observed for the high intensity of the $^4F_{9/2} \rightarrow {}^4I_{15/2}$ transition. The probable mechanism that takes the high intensity of the red emission is shown in Fig. 8b. The absorption 808 nm radiation results in the $^4I_{11/2}$ (Er) level. The predominance of the red emission in relation to green emission has been observed by Wang [22] in vitro ceramic host. The ESA approach

Table 7 The emission bands against the intra f–f transitions of powder and thin film form BT samples doped with Er^{3+} and Yb^{3+} ions

Emission bands positions (nm)	Intra f–f transitions
Powder form	
532	$^2H_{11/2} \rightarrow {}^4I_{151/2}$
550	$^4S_{3/2} \rightarrow {}^4I_{151/2}$
634.5	$^4F_{97/2} \rightarrow {}^4I_{11/2}$
Thin film form	
505	$^2H_{11/2} \rightarrow {}^4I_{151/2}$
532	$^4S_{3/2} \rightarrow {}^4I_{151/2}$
635	$^4F_{97/2} \rightarrow {}^4I_{11/2}$

occurs only during excitation, whereas the ET can happen both during and after excitation.

3.1.2 *Up-conversion emission of BT: Er^{3+}, Yb^{3+} ions*

The up-conversion effect observed in BT powder and thin film forms doped with constant concentration of Er^{3+} ions and different concentrations of Yb^{3+} ions is shown in Fig. 9 (a) (BT4E1Y, and (b) (BT4E4Y), and Fig. 10 (a) (BT4E2YTF), (b) (BT4E4YTF) and (c) (BT4E5YTF), respectively. While the Schematic diagram of the electronic levels of both systems (Er^{3+} and Yb^{3+}) incorporated into BT nano-structure spin coating thin film and powder samples, is shown in Fig. 11. The obtained emission bands observed in Figs. 9 and 10 in both systems are attributed to the intra f-f transitions of Er^{3+} and Yb^{3+} ions, corresponding to green and red emissions. It is clearly seen that the intensity of the emission is stronger and broader in powder sample than in thin film one. The emission bands observed at 532 nm ($^2H_{11/2} \rightarrow {}^4I_{15/2}$), 550 nm ($^4S_{3/2} \rightarrow {}^4I_{15/2}$) and 634.5 nm ($^4F_{9/2} \rightarrow {}^4I_{15/2}$) (for powder) and the

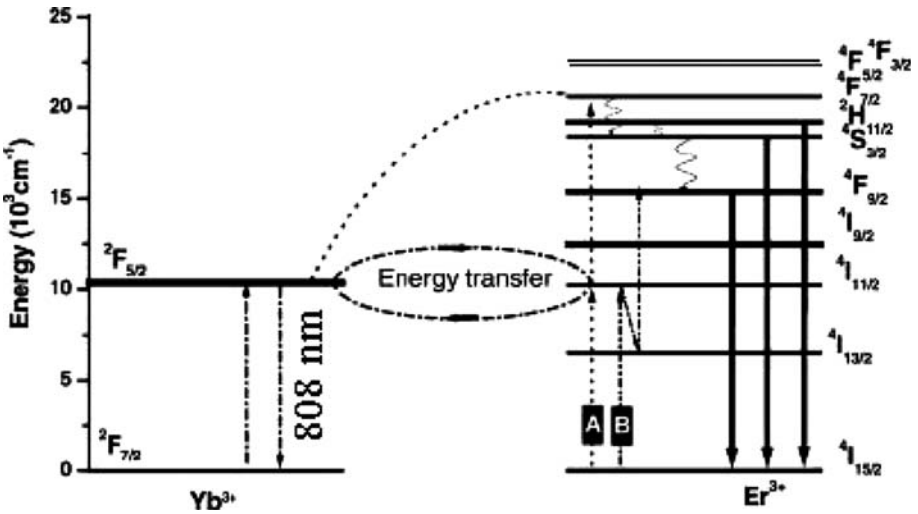

Fig. 11 Schematic diagram of the electronic levels of Er^{3+}: Yb^{3+} ions co-doped into BT in powder and thin film forms. The *solid lines arrows* indicate the emission transitions for Er^{3+} ion. The *wavy lines* represent the non-radiative process. The *dash dot lines* represent the absorption transition for the Er^{3+} and Yb^{3+} ions. The process (*A*) represent excitation through energy transfer while (*B*) represents excitation through excited state absorption

other emission bands at 505 nm ($^2H_{11/2} \rightarrow {}^4I_{15/2}$), 532 nm ($^2H_{11/2} \rightarrow {}^4I_{15/2}$) and 635 nm ($^4F_{9/2} \rightarrow {}^4I_{15/2}$) (for thin film), are attributed to the intra f-f transitions of Er^{3+} and Yb^{3+} ions, where the red emission is attributed to another f-f transition of Er^{3+} and Yb^{3+} ions for both form of samples, respectively as shown in Table 7. These transitions are possible due to an efficient energy transfer process involving Er^{3+} and Yb^{3+} ions identical to the one discussed by Hewes and Server [16]. After Yb^{3+} absorption, the excitation energy can be transferred to the $^4I_{11/2}$ Er^{3+} level, via the cross-relaxation mechanism: $^2F_{5/2} \rightarrow {}^2F_{7/2}$ (Yb^{3+}) and $^4I_{11/2} \rightarrow {}^4I_{15/2}$ (Er^{3+}), as depicted schematically in the diagram of Er^{3+} and Yb^{3+} ion levels shown in Fig. 11. Additionally, a second cross-relaxation from Yb^{3+} to a previously excited Er^{3+} ion leads to the excitation of the Er^{3+} ion to higher levels via the new transfer processes: $^2F_{5/2} \rightarrow {}^2F_{7/2}$ (Yb^{3+}) and $^4I_{15/2} \rightarrow {}^4I_{11/2}$ (Er^{3+}) [17].

4 Conclusion

Pure BT powder and co-doped with Er^{3+} and Yb^{3+} ions, were successfully synthesized via sol gel technique. Sintering of the thin film and powder samples at 750 °C for 1 h resulted in tetragonal phases, as confirmed by XRD analysis. Structural study revealed that the average crystallite sizes were found to be dependent on the concentrations of erbium, as it decreases from 38 to 37 nm by increasing the concentration of Er^{3+} ions.

Efficient infrared-to-visible up- conversion in BT: Er^{3+} and BT: Er^{3+}, Yb^{3+} co-doped powder and thin film samples were observed, and its origin was investigated. The $^4F_{9/2}$ is predominantly excited in the BT samples doped with Er^{3+} ions in both forms of preparation. Green and red luminescent emissions resulting from the doped BT sample with erbium ions and co-doped it with erbium and ytterbium ions in powder and thin film forms. It is clearly seen that the thin film has sharper up-conversion emission band than the powder sample by doping them by Er^{3+} ions and co-doped them by Er^{3+} and Yb^{3+} ions.

References

1. Battisha IK, El Beyally A, Abd El Mongy S, Nahrawi AM (2007) J Sol Gel Sci Technol 41:129
2. Battisha IK (2007) J Non Cryst Solids 353:1748
3. Zhang HX, Kan CH, Zhou Y, Han XQ, Buddhudu S, Xiang Q, Lam YL, Chan CW (2000) Appl Phys Lett 77(5):609
4. Iparraguirre I, Azkargorta J, Fernandez-Navarro JM (2007) J Non Cryst Solids 353:990
5. Battisha IK, Afify HH, Badr Y (2002) J Sol Gel Sci Technol 25:5
6. Badr Y, Salah A, Battisha IK (2005) J Sol Gel Sci Technol 34:219
7. Zhang HX, Kam CH, Zhou Y, Han XQ, Lam YL, Chan YC, Pita K (2000) J Mater Chem Phys 2:174
8. Zhang HX, Kan CH, Zhou Y, Han XQ, Buddhudu S, Xiang Q, Lam YL, Chan CW (2000) J Appl Phys Lett 77(5):609
9. Chiasera A, Tosello C, Moser E, Montagna M, Belli R, Gonçalves RR, Righini GC, Pelli S, Chiappini A, Zampedri L, Ferrari M (2003) J Non Cryst Solids 322:289
10. Hoerman BH, Ford GM, Kaufmann LD, Wessels BW (1998) J Appl Phys Lett 73:2248
11. Yoon SG, Safari A (1995) Thin Solid Films 254:211
12. Zhigang S, Weiwei Z, Jianfeng C, Yun J (2006) Chin J Chem Eng 14(5):642
13. Battisha IK (2004) J Sol Gel Sci Technol 30:163
14. Som T, Karmakar B (2009) J Alloys Compd 476:383
15. Badr Y, Salah A, Battisha IK (2005) J Sol Gel Sci Technol 34:219
16. Hewes RA, Server JF (1968) Bull Am Phys Soc 13:687
17. Yanagisawa K, Ovenstone J (1999) J Phys Chem B103:7781
18. Li B, Wang X, Li L (2003) J Mater Chem Phys 78(1):292
19. Yao K, Zhu W (2002) Thin Solid Films 408(1–2):11
20. Yao Z, Liu H, Liu Y, Wu Z, Shen Z, Liu Y, Cao M (2008) J Mater Chem Phys 109:475
21. Paris EC, Gurgel MFC, Bosehi TM, Joya MR, Pizan PS, Souza AG, Leie ER, Varela JA, Longo E (2008) J Alloys Compd 462:157
22. Wang Y, Ohwaki J (1993) J Appl Phys Lett 63:3268